Monolayer of Mie-Resonant Silicon Nanospheres for Structural Coloration

Tanaka, Haruki
Hotta, Shinnosuke
Hinamoto, Tatsuki
Sugimoto, Hiroshi
Fujii, Minoru

(Citation)
ACS Applied Nano Materials,7(3):2605-2613

(Issue Date)
2024-01-29

(Resource Type)
journal article

(Version)
Accepted Manuscript

Monolayer of Mie-Resonant Silicon Nanospheres for Structural Coloration

Haruki Tanaka, Shinnosuke Hotta, Tatsuki Hinamoto, Hiroshi Sugimoto, Minoru Fujii***

Department of Electrical and Electronic Engineering, Graduate School of Engineering, Kobe University, 1-1 Rokkodai, Nada, Kobe 657-8501, Japan

*e-mail: sugimoto@eedept.kobe-u.ac.jp

**e-mail: fujii@eedept.kobe-u.ac.jp

KEYWORDS: monolayer, Mie resonance, Langmuir-Blodgett method, printed nanosphere

Abstract

Structural coloration of a monolayer of Mie-resonant silicon (Si) nanospheres (NSs) produced by a solution-based process is studied. It is shown by simulation that a monolayer of hexagonal close-packed Si NSs exhibits size-dependent structural color with the peak reflectance of ~50 %. The peak reflectance can be increased to over 90 % by introducing spaces between Si NSs. The high reflectance despite the small coverage is due to the very high scattering efficiency of Mie-resonant Si NSs. Monolayers of densely-packed Si NSs are produced from Si NS suspensions by the Langmuir-Blodgett (LB) method. The monolayers exhibit size-dependent structural color with the

peak reflectance of 30-50 %. The color is very insensitive to the viewing angle, and the angle dependence of the reflectance spectra is very small. The peak reflectance is increased by increasing the distance between NSs by partially oxidizing the layers. The results demonstrate that iridescence-free structural coloration of a substance is possible by a layer of Si NSs much thinner than the monolayer, i.e., by sparsely scattered Si NSs.

1. Introduction

Crystalline silicon (Si) has a very high refractive index ($n \approx 4$) and a small extinction coefficient in the visible range, and thus the nanoparticle (NP) exhibits sharp Mie resonances in the visible range when the diameter is in 100-200 nm range.[1–6] The scattering efficiency at the resonance wavelength is very high (~10) and thus the scattering is much brighter than that of plasmonic NPs such as gold and silver NPs with comparable sizes.[2,7–9] Different from plasmonic NPs in which the resonance wavelength, i.e., scattering color, is predominantly determined by the shape, that of Mie-resonant Si NPs is very sensitive to the size, and thus the color can be easily tuned by the size.[2] Because of these properties, Si NPs have been considered as a promising component for structural coloration.[10–16] Since Mie scattering of individual NPs is the origin of the color, very high resolution painting (~100,000 dpi) is in principle possible.[12,13] Furthermore, because of the large tunability of the resonance wavelength, wide color gamut can be achieved. It is often wider than that achieved in plasmonic NPs.[17–21] Coloration by Si NPs has been discussed not only for the regularly-aligned structures,[22,23] but also for randomly-distributed structures.[22,24,25]

To realize structural coloration by Si NPs, both the top-down and bottom-up approaches have been developed. The former one is using nano-fabrication technology such as electron beam

lithography (EBL) and reactive ion etching to produce Si NPs with desired size and shape at desired positions on a substrate.[12–16,26–28] The latter approach uses Si NPs as a color pigment (color ink) that can be painted on a base material. This approach is more versatile than the former one and has applications in wider fields. The crucial issue of this approach is the production of high quality inks in which Si NPs with uniform size and shape are dispersed without agglomeration. Si NP inks satisfying these requirements had been hard to be produced by conventional processes such as plasma synthesis,[29–31] chemical vapor deposition,[32,33] laser ablation,[2,7,34–39] and mechanical milling.[40,41] In previous work,[10,11,42–44] we developed a process to produce suspensions of almost perfectly spherical Si NPs (Si nanospheres (Si NSs)) with very narrow size distributions. The suspension exhibited size-dependent vivid structural color due to the Mie resonance.[10,42,43] By mixing the suspension with an optically transparent binder such as polyvinylpyrrolidone (PVP), we produced the structural color inks and demonstrated coloration of a base material such as a PET film by painting.[10]

Considering the very high scattering efficiency of Mie-resonant Si NSs, a very small amount is required for coloration of a substance. For example, a monolayer of Si NSs is expected to have reflectance high enough for coloration. In this work, we study theoretically and experimentally the light reflection property of Si NS monolayers. First, we study reflection properties of hexagonal close-packed Si NS monolayers formed on a silica substrate by numerical simulation. We show that coloration of silica substrates is possible by a Si NS monolayer and the peak reflectance can be around 50 %. We also show that the reflectance increases by introducing space between Si NSs in an array, and the maximum reflectance can be over 90 %.

We then produce Si NS monolayers on silica substrates by Langmuir-Blodgett (LB) method from the suspensions of size-separated Si NSs. Scheme 1 shows the outline of the procedure. First, we produce NSs of crystalline Si by disproportionation reaction of silicon monoxide (SiO) and disperse them in methanol. The NSs are then separated in size and Si NS structural color inks are produced. Finally, Si NS monolayers are produced on a silica substrate by the LB method. We show that the Si NS monolayers exhibit size-dependent vivid structural color with the peak reflectance of 30-50 %. The color is very insensitive to the viewing angle. We also experimentally study the effect of NS-to-NS distance on the reflection property by partially oxidizing the densely-packed Si NS monolayers. Throughout this work, we demonstrate that iridescence-free structural coloration of a substance by a layer of Si NSs much thinner than the monolayer, i.e., by sparsely scattered Si NSs, is possible by a solution-based process.

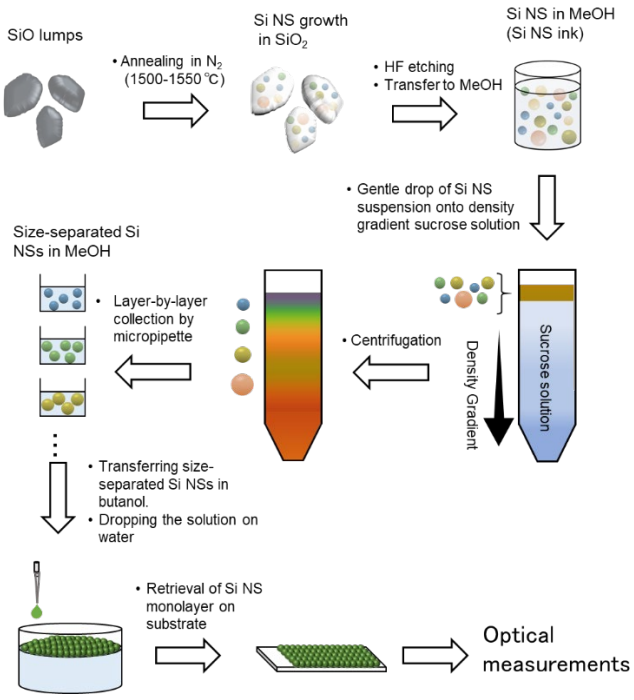

Scheme 1

Procedure for the preparation of a monolayer of size-separated Si NSs.

2. Results and Discussion

2.1. Reflection property of Si NS monolayers (simulation)

Figure 1a shows the scattering cross-section spectrum of a single Si NS 150 nm in diameter in vacuum. The spectrum is composed of the magnetic dipole (MD) and electric dipole (ED) Mie resonances. Figure 1b shows calculated reflectance spectra of hexagonal close-packed Si NS monolayers on silica substrates. Incident light is normal to the surface, and light reflected to the upper hemisphere is monitored, i.e., both the specular and diffuse reflectance are involved in the spectra. The diameter (d) of Si NSs is changed from 100 nm to 200 nm. If we compare the scattering spectrum of a 150 nm-diameter Si NS in Figure 1a with the reflectance spectrum of a monolayer of the same size Si NSs (green solid curve in Figure 1b), they are very much different. The reflectance spectrum oscillates like an interference fringe, although a broad reflectance peak appears around the MD and ED Mie resonance wavelengths. On the reflectance spectrum, a spectrum calculated by assuming a uniform thin film with an effective refractive index obtained from the effective medium theory (Si : air = 0.605 : 0.395) is overlapped (red dashed curve) (see Supporting Information for more details). The spectrum calculated by assuming the uniform effective medium has some similarities with the simulated spectrum. This suggests that the overall response of a hexagonal close-packed Si NS monolayer to a plane wave is close to that of a uniform effective medium, although the signature of the Mie resonance remains as a reflection peak around the MD and ED resonance wavelengths.

In Figure 1b, the reflectance peak shifts to longer wavelength with increasing the Si NS diameter, and in all the sizes, the peak reflectance reaches ~50 %. This large reflectance value indicates that the Si NS monolayers can be used for structural coloration despite the very thin thickness. The

chromaticity diagram in Figure 1c shows that the color can be controlled by Si NS diameter, although the color saturation is low because of the interference-like multiple peaks in the reflectance spectra.

Figure 1d shows the reflectance spectra of Si NS hexagonal arrays with space between NSs. The diameter of Si NSs is fixed to 150 nm. In each graph, a corresponding volume filling factor (*f*) is shown together with the surface-to-surface distance (*g*). The spectrum with $g = 0$ nm is the same as that in Figure 1b ($d = 150$ nm). Introduction of a small gap modifies the spectral shape significantly. The interference-like oscillation almost completely disappears already when $g = 50$ nm, and only a broad reflection band remains around the MD and ED Mie resonance wavelengths. Further increase of the gap results in the appearance of the distinctive MD and ED peaks in the reflectance spectra. Interestingly, introduction of spaces between NSs results in the increase of the peak reflectance despite the decrease of the volume filling factor of Si NSs. The green squares in Figure 1e show the peak reflectance value as a function of *f*. It increases significantly and reaches 93 % for $f = 34$ % ($g = 50$ nm). Although further increase of the gap results in the decline of the peak reflectance, it is over 70 % even for $f = \sim 10$ % ($g = 210$ nm). This high reflectance despite small coverage of the surface by Si NSs is due to the very large scattering efficiency.[2,5,7,10,11,22] Similar data are obtained when Si NSs are embedded in different medium, e.g., in SiO_2 (see Figure S2 in Supporting Information). The requirement of very small amount of Si NSs for coloration is an advantage in the application as a color pigment.

In actual Si NS monolayer samples we will discuss later, Si NSs are not perfectly aligned. Therefore, we also calculated the reflectance spectra of 2D random arrays of Si NSs (Figure S3 in Supporting Information). The blue circles in Figure 1e show the data obtained for the random array. The peak reflectance of the random array is lower than the hexagonal array. However, the

reflectance of over 50 % is possible when *f* is larger than 20 %. In the case of uniform thin films with the effective refractive indices (red triangles in Figure 1e), the reflectance decreases monotonously with decreasing the filling factor. Therefore, Si NS hexagonal arrays with space between the NSs cannot be treated as uniform thin films with effective refractive indices.

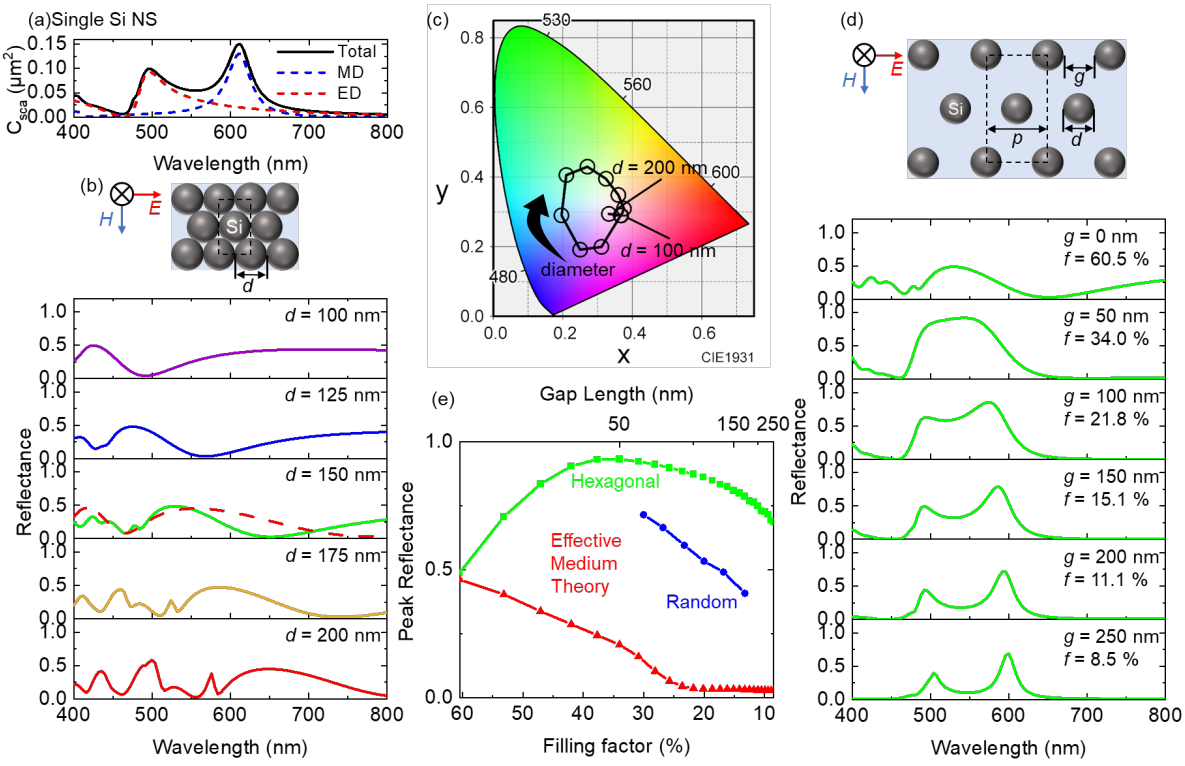

Figure 1. (a) Calculated scattering cross-section spectrum of a single Si NS with 150 nm in diameter in vacuum. The components of the magnetic dipole (MD) and electric dipole (ED) modes are shown by blue and red broken curves, respectively. (b) Calculated reflectance spectra of hexagonal close-packed Si NS monolayers on silica substrates. Incident light is normal to the surface, and light reflected to the upper hemisphere is monitored, i.e., both the specular and diffuse reflectance are involved in the spectra. The diameter (*d*) of Si NSs is changed from 100 nm to 200 nm. On the spectrum of a Si NS monolayer composed of 150 nm-diameter Si NSs, the spectrum

calculated by assuming a uniform thin film with an effective refractive index obtained from the effective medium theory (Si : air = 0.605 : 0.395) is shown with a dashed curve. (c) Chromaticity diagram (CIE 1931) of hexagonal close-packed Si NS monolayers on silica substrates. The diameter is changed from 100 nm to 200 nm. (d) Reflectance spectra of Si NS hexagonal array monolayers. The diameter of Si NSs is fixed to 150 nm and the surface-to-surface distance (*g*) is changed from 0 to 250 nm. The volume filling factor (*f*) is shown in the graphs. Both the specular and diffuse reflectance are involved in the spectra. (e) Peak reflectance values as a function of *f*. The data obtained for hexagonal array (green squares) and random array (blue circles) monolayers of Si NSs and those obtained for uniform thin films with effective refractive indices (red triangles) are shown. Corresponding surface-to-surface distance (*g*) in the case of hexagonal array is shown in the upper axis.

2.2. Structural coloration by Si NS monolayers

(a) Monolayers of Si NSs with broad size distribution

We prepare Si NS monolayers from Si NS suspensions. The preparation procedure of the suspension is briefly described in the Experimental Section, and the details are found in our previous papers.[10,11,42] Figure 2a shows a methanol suspension of Si NSs before size purification. The NS concentration (*C*) is 736 μg/mL. The color is brownish and the extinction spectrum (Figure 2b) is very broad due to the broad size distribution. Figure 2c shows the TEM image. The NSs are almost perfectly spherical. The average diameter estimated from the TEM image is about 150 nm.

Si NS monolayers are produced by LB method as schematically shown in Figure 2d (see Experimental Section). The size of a silica substrate is 2 cm×1 cm and a Si NS monolayer is formed in a 1.5 cm×1 cm area. Figure 2e shows a photograph of a Si NS monolayer on a silica substrate

under white LED illumination. The background of the area surrounded by broken lines is a contrast ratio test paper. The color difference between the white and black background is very small indicating that the Si NS monolayer hides the background color effectively. We compare the transmittance and reflectance spectra of the Si NS monolayer with that of a TiO_2 NP monolayer, which are known to have high hiding power[45] and used as sunscreen and for cosmetics. Figure 2f shows the photo of a TiO_2 NP (200 nm in diameter) (Ishihara Sangyo Kaisha) monolayer produced by the same procedure as the Si NS monolayer. By comparing two photos, we can see that Si NSs more effectively hides the background, although the brownish color may limit the application. This can be qualitatively evaluated by the regular transmittance spectra (Figure 2g). The regular transmittance of the Si NS monolayer is smaller than that of the TiO_2 NP monolayer in a wide wavelength range and is smaller than 10 % in the whole visible range. Figure 2h, 2i and 2j shows the specular, diffuse and total reflectance spectra of the Si NS and TiO_2 NP monolayers. The specular reflectance is very small in both samples, and thus the reflectance is almost solely the diffuse reflectance. The reflectance of the Si NS monolayer in 400-700 nm range is smaller than that of the TiO_2 NP monolayer due to the absorption loss, while that above 700 nm is larger due to the higher refractive index and the existence of the MD and ED Mie resonance peaks in the wavelength range (see scattering cross-section spectra of a TiO_2 NP and a Si NS in Figure S4 in Supporting Information).

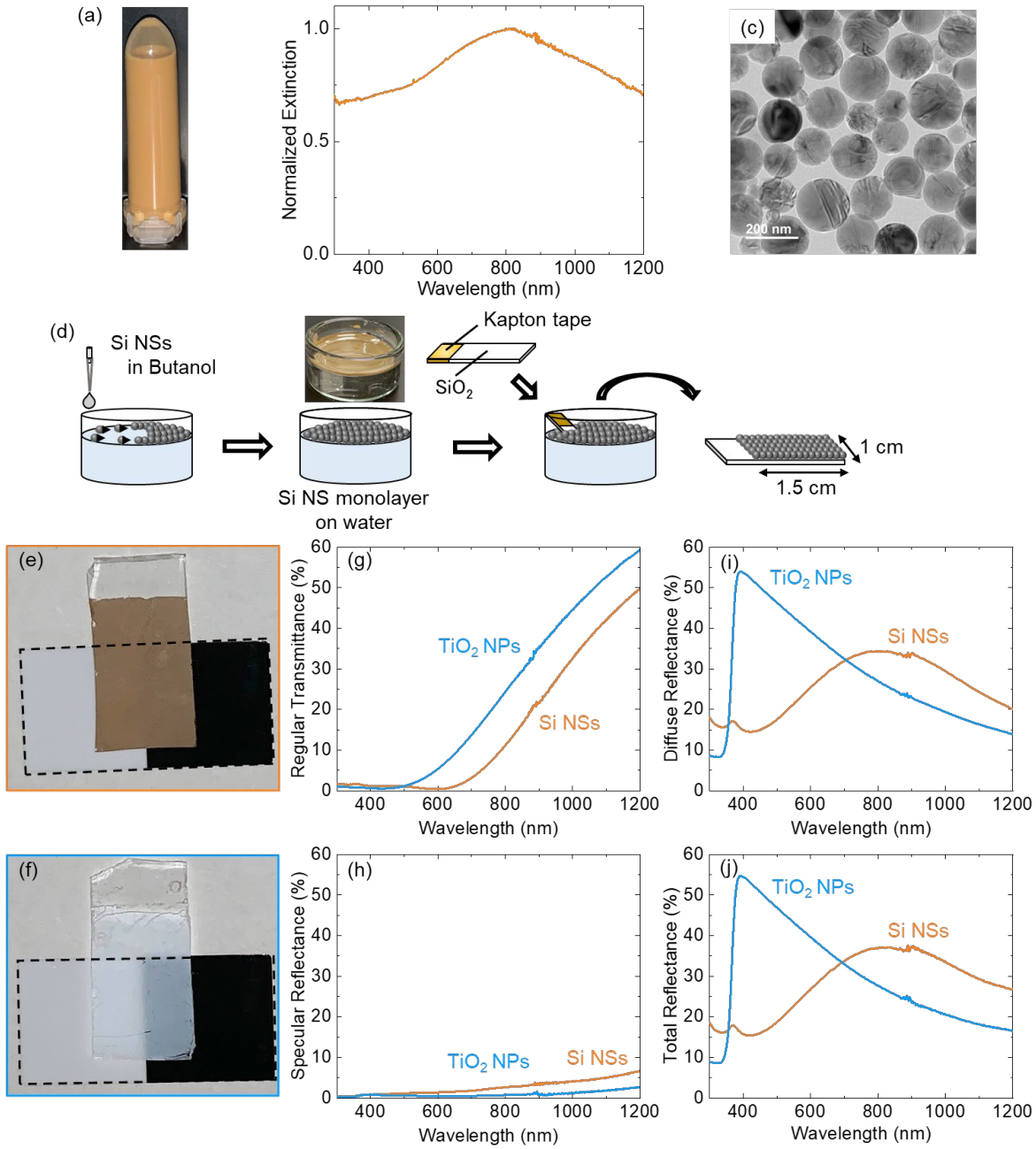

Figure 2. (a) Photograph of methanol suspension of Si NSs with broad size distribution. (b) Extinction spectrum of the suspension in (a). (c) Typical TEM image of Si NSs. (d) Schematic illustration of the procedure to produce a Si NS monolayer. The photograph is a water-filled petri dish with a Si NS monolayer at the air/water interface. (e, f) Photographs of a Si NS monolayer (e) and a TiO_2 NP monolayer (f) on a silica substrate under white LED illumination. The

background area surrounded by broken lines is a contrast ratio test paper. (g) Regular transmittance spectra of the Si NS and TiO_2 NP monolayers. (h-j) Specular reflectance (h), diffuse reflectance (i), and total reflectance (j) of the Si NS and TiO_2 NP monolayers. The total reflectance spectra are the sum of the specular and diffuse reflectance spectra.

(b) Monolayers of Si NSs with narrow size distribution

The brownish suspension of Si NSs in Figure 2a can be separated into those containing Si NSs with specific sizes.[10,11,42,43] Figure 3a shows the photos of methanol suspensions of size-purified Si NSs, and Figure 3b shows the extinction spectra. Below the photos in Figure 3a, the average diameter (d_{ave}) and the coefficient of variation of the size distribution (C_v) defined by the standard deviation (σ) divided by d_{ave} estimated from the extinction spectra are shown (see Supporting Information for details) together with the NS concentration (C). Because of the small C_v, vivid structure color can be seen in the suspensions. The color of the suspension of the smallest size Si NSs is pink (not blue). This is due to the multiple scattering, i.e., blue light subsides during consecutive scattering by absorption, while red light survives.[11] In diluted suspensions of Si NSs, the scattering color changes progressively from blue to orange with increasing the size.[42,43]

Figure 3c shows the photos of Si NS monolayers produced from the suspensions in Figure 3a by the procedure shown in Figure 2d under white LED illumination. The background is a black paper. Structural coloration of silica substrates from violet to yellow can be seen. Figure 3d shows the photos of the same samples taken from a 45° direction. The color does not change. This can be seen in the angle-dependence of the reflectance spectra in Supporting Information (Figure S7). The viewing angle insensitiveness is due to the fact that the color originates from Mie resonances of individual Si NSs. This is an advantage of this method for structural coloration compared to

those using periodic structures. Figure 3e shows a typical SEM image (d_{ave} = 151 nm). A Si NS monolayer is formed except for small regions of voids and agglomerates. We can see domains of hexagonal closed pack structures, although the domain size is small. The domain size may be increased by further reducing the size distribution. Figure 3f, 3g and 3h shows the specular reflectance, diffuse reflectance and total reflectance, respectively, spectra of the Si NS monolayers. In contrast to the Si NS monolayer with a broad size distribution (Figure 2h-j), both the specular and diffuse reflectance spectra have distinctive peaks. The specular reflectance spectra have interference-like oscillation and are similar to the simulated spectra in Figure 1b. The total reflectance spectra have single broad peaks and the peak shifts from 448 nm to 741 nm when d_{ave} is changed from 111 nm to 228 nm. The reflectance exceeds 30 % in all the samples and it reaches 48 % in the largest size one. Figure 3i shows the chromatic diagram obtained from the total reflectance spectra in Figure 3h. We can see the change of the color, although the saturation is lower than the simulation data in Figure 1c. This may be due to the finite size distributions of Si NSs and the disorder in the alignment.

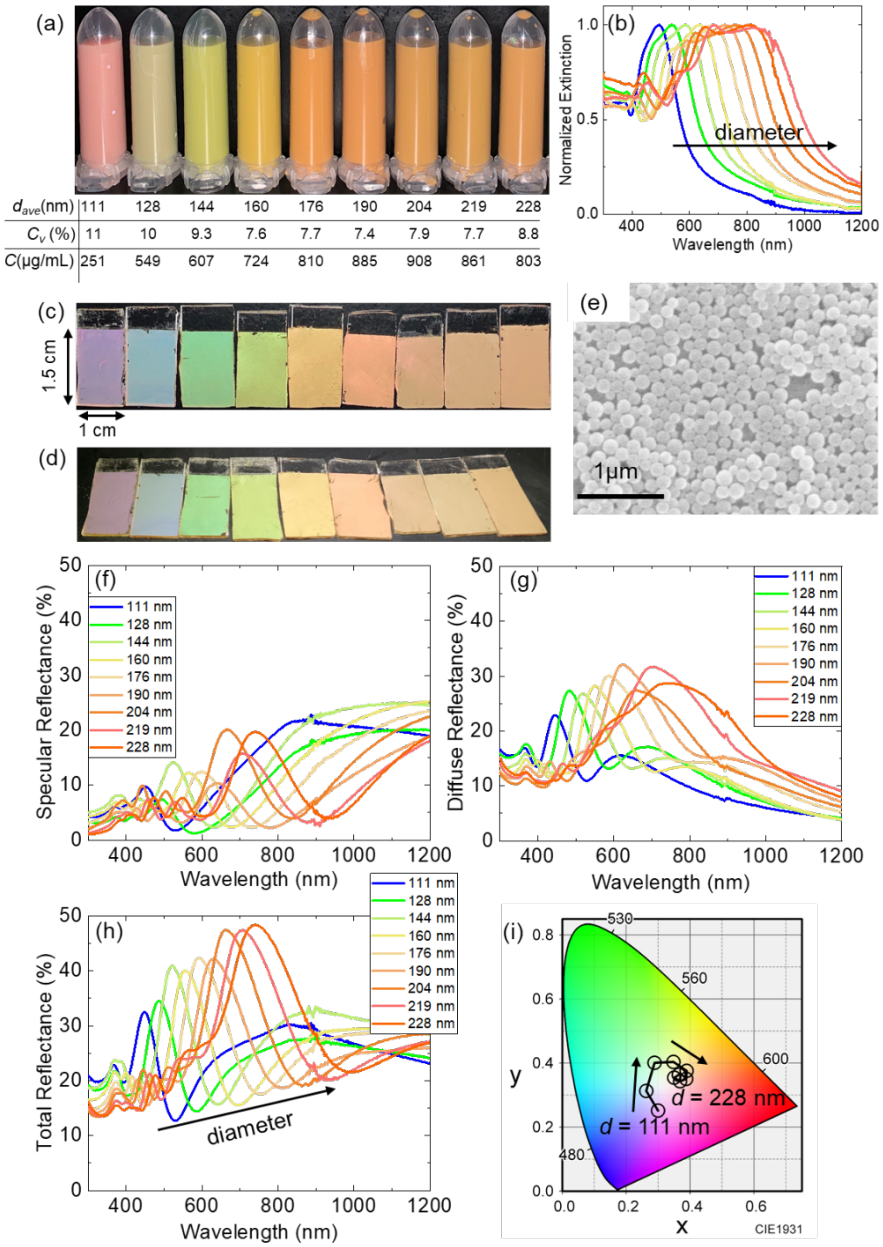

Figure 3. (a) Photographs of methanol suspensions of size-purified Si NSs. The average diameter (d_{ave}), the coefficient of variation (C_v) of the size distribution, and the concentration (C) are shown below the photographs. (b) Extinction spectra of Si NS suspensions in (a). (c, d) Photographs of Si NS monolayers on silica substrates taken from the normal to the surface (c) and from a 45° direction (d). (e) Typical SEM image of a Si NS monolayer (d_{ave} = 151 nm). (f-h) Specular reflectance (f), diffuse reflectance (g) and total reflectance (h) spectra of Si NS monolayers in (c).

The total reflectance spectra are the sum of the specular and diffuse reflectance spectra. (i) Chromaticity diagram (CIE 1931) of Si NS monolayers. The average diameter is changed from 111 nm to 228 nm.

(c) Oxidation of monolayers of Si NSs with narrow size distribution

In Figure 1d, we showed by simulation that introducing space between Si NSs in a close-packed monolayer improves the coloration performance, especially the peak reflectance. In order to imitate that, we partially oxidized the Si NS monolayers. The oxidation temperature is fixed to 1100 ℃, and the oxide thickness is controlled by the oxidation duration (Figure S8 in Supporting Information). Figure 4a shows a TEM image of a Si NS (d_{ave} = 150 nm) oxidized for 16 min. SiO_2 layers of about 34 nm in thickness are grown by oxidation. In Supporting Information (Figure S9), we show calculated scattering cross-section spectra of a Si NS with a SiO_2 shell. The ED mode is affected more by the shell than the MD mode and is broadened.

Figure 4b shows photos of Si NS monolayers after oxidation for different durations (0-74 min). The background is a black paper. We can clearly see the change of the color by oxidation. In small Si NSs, the color disappears after 74 min oxidation due to full conversion of Si NSs to silica NSs. On the other hand, in large Si NSs, structural color appears after oxidation due to the shift of the Mie resonances from the near-infrared range to the visible range.

In Figure 4c, the reflectance spectra of a Si NS monolayer with the initial diameter of 211 nm after oxidation for different durations are shown. After 3 min oxidation, the peak shifts from 703 nm to 652 nm. This is due to the reduction of the size of a Si NS core by oxidation. In general, size reduction decreases the scattering cross-section at the resonance. However, despite the decrease of the scattering cross-section, the reflectance increases by oxidation for 3 min. This is due to opening

the space between Si NSs by oxidation, and is consistent with the simulation data in Figure 1e. In Figure 4c, the spectral shape does not change significantly even if the space between Si NSs increases by oxidation. This is not the same in Figure 1e, where distinctive Mie resonances appear after opening the gap between NSs. The almost featureless reflectance spectra after oxidation in Figure 4c may be due to size distribution of Si NSs and randomness of the alignment. In Figure 4d, the relation between the peak reflectance and the peak wavelength is shown for Si NSs with different initial diameters and for different oxidation durations (corresponding reflectance spectra in Supporting Information (Figure S10)). Similar behavior, i.e., the initial increase of the reflectance by oxidation, is observed for all the samples.

The partially-oxidized Si NS monolayers are modeled as hexagonal close-packed structure of Si NS core/silica shell NSs. In Supporting Information (Figure S11), calculated reflectance spectra of the monolayer core/shell NSs are shown. The simulation suggests that color saturation larger than that of Figure 1c is expected if the hexagonal alignment of the core/shell NSs is realized, although the actual samples in Figure 4 cannot fully enjoy the benefit because of the remaining size distribution and the randomness of the NS alignment.

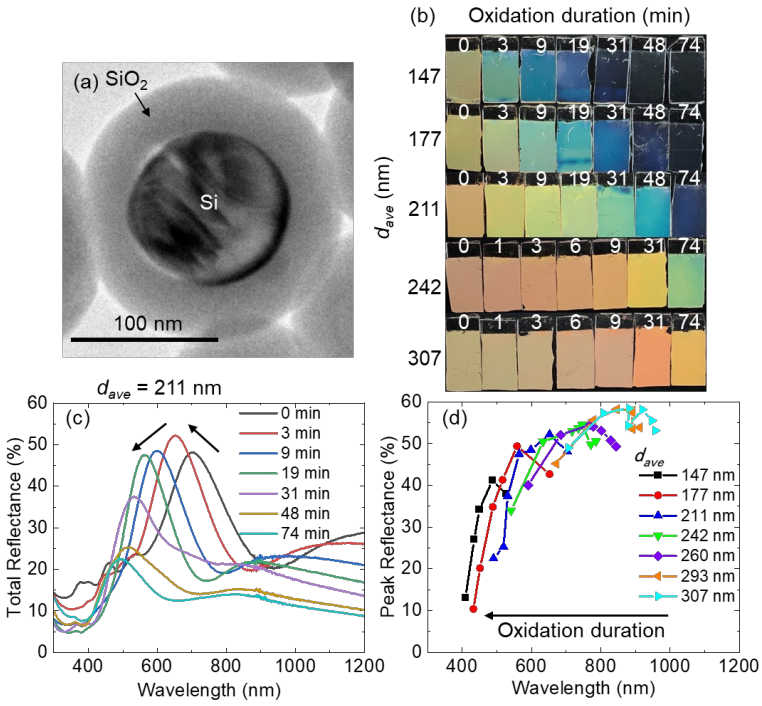

Figure 4. (a) TEM image of a Si NS oxidized at 1100 ℃ for 16 min in air. (b) Photographs of Si NS monolayers before and after oxidation. The horizontal axis is the oxidation duration, and the vertical axis is the average diameter of Si NSs before oxidation (d_{ave}). (c) Reflectance spectra of a Si NS monolayer (d_{ave} = 211 nm) before and after oxidation. The oxidation duration is changed from 0 to 74 min. (d) Peak reflectance value of Si NS monolayers as a function of the peak wavelength. The average diameter of Si NSs (d_{ave}) is changed from 147 nm to 307 nm. The oxidation duration is changed from 0 to 74 min.

3. Conclusion

We study the capability of Si NS monolayers for structural coloration of a substance. Numerical simulation reveals that hexagonal close-packed Si NS monolayers exhibit size-dependent structural color and the peak reflectance reaches 50 %. The peak reflectance increases to over 90 % by introducing space between Si NSs in an array. Even when the volume filling factor of Si NSs

on substrate surface is 10 %, peak reflectance can be over 70 %. The high reflectance despite the small coverage is due to the very high scattering efficiency of Mie-resonant Si NSs. This allows us to reduce the amount of materials necessary for coloration and is an advantage in the practical applications as a color pigment.

We then produce monolayers of densely-packed Si NSs from the suspensions by LB method. Si NS monolayers produced from size-purified suspensions exhibit size-dependent structural color with the peak reflectance of 30-50 %. Although these values are slightly smaller than the values calculated for hexagonal close-packed structure, the results demonstrate that structural coloration is possible by Si NS monolayers by a solution-based process. The color is very insensitive to the viewing angle. Finally, we study the effect of space between Si NSs in an array on the reflection property by partially-oxidizing densely-packed Si NS monolayers, and show that introduction of space between NSs increases the peak reflectance. The experimental demonstration of iridescence-free structural coloration of a substance by a layer of Si NSs much thinner than the monolayer, i.e., by sparsely scattered Si NSs, is an important progress in the development of Si NS-based color pigments.

4. Experimental Section

Preparation of Si NS suspensions: Si NSs were prepared by thermal disproportionation of silicon monoxide (SiO) lumps.[10,11] SiO lumps (several mm in size) (FUJIFILM Wako, 99 %) were annealed at 1500-1550 ℃ in a N_2 gas atmosphere for 30 min to grow crystalline Si NSs in silica (SiO_2) matrices. Si NSs were liberated from SiO_2 matrices by etching in HF solution (46 wt.%) for 1 h. Liberated Si NSs were transferred to methanol by the following process. Methanol was added to HF solution of Si NSs, and the mixture solution was subjected to centrifugation for 1 min to

precipitate Si NSs. After removing the supernatant liquid, methanol was added to the tube and Si NSs were redispersed. The centrifugation and the solution exchange were repeated several times until the pH of the solution became 4-6. Finally, Si NSs were subject to sonication in methanol with an ultrasonic homogenizer (Violamo SONICSTAR 85).

Size Separation of Si NSs: Sucrose density gradient centrifugation process was employed for size separation of Si NSs.[5,11] Sucrose density gradient solution was prepared by carefully adding 2.2 ml sucrose solution at six different concentrations (55-42.5 wt.%, 2.5 wt.% increments) to a 15 ml centrifugal tube in order. Methanol suspension of Si NSs (1.8 ml) was added to the top of the tube, and the tube was the subject of centrifugation at 5500 rpm for 55-60 min to form layers of size-separated Si NSs. The layers were retrieved 1 ml at a time from the top and transferred to different tubes. The suspensions of size-separated Si NSs were washed with water several times to remove sucrose and transfer to methanol.

Fabrication of Si NSs monolayer: Si NS monolayers were fabricated by LB method (Figure 2d). First, the surface of Si NSs was etched in HF solution (5 wt.%) for 2 min to make the surface hydrophobic, and then they were transferred to butanol. The butanol suspension of Si NSs was slowly dropped onto the surface of water in a petri dish to form the monolayer at the air/water interface (Figure S6 in Supporting Information). Finally, the monolayer was transferred to a SiO_2 substrate (1.5 cm×1 cm).

Optical characterization: Specular reflectance spectra were measured by a double-beam spectrophotometer (UV-3101PC, Shimadzu) with the incident and detection angle of 5°. The diffuse reflectance spectra were measured by a double-beam spectrophotometer equipped with an integrating sphere (Spectrapro3700, Shimadzu). The size of incident light at the sample point was 6×10 mm^2. Incident light was randomly polarized in both measurements.

Numerical Simulation: The FDTD simulations of 2D hexagonal and random arrays of Si NSs were carried out using a commercial software (Lumerical, Ansys). The periodic boundary conditions were used for the *x*- and *y*-directions and the perfectly matched layer (PML) boundary was used for the *z*-direction. For the generation of a random array, a uniform random particle distribution object in the package was used. The mesh size was 5 nm and the thickness of PML was about 250 nm. The structure was illuminated by a plane wave polarized along the *x*-axis in Figure 1a from the normal to the surface. Reflection spectra were obtained by 2D power monitor. The complex dielectric permittivity of Si and SiO_2 was taken from Palik's book.[46] The thickness of a SiO_2 substrate was assumed to be infinite.

Calculation of Scattering Spectrum of single Si NS: A scattering cross-section spectrum of a Si NS in air was calculated using the analytical equations of the Mie theory.[47,48] The complex permittivity of Si crystal taken from Palik's book[46] was used.

Supporting Information

The Supporting Information is available free of charge at https://pubs.acs.org/doi/

1. Calculation of the reflectance spectrum of a Si NS monolayer under the assumption that the layer is a uniform thin film with the refractive index obtained from the effective medium theory, 2. Calculated reflectance spectra of 2D hexagonal array of Si NSs in SiO_2, 3. Calculated reflectance spectra of 2D random array of Si NSs on a silica substrate, 4. Calculated scattering cross section spectra of single Si NS and TiO_2 NP, 5. Estimation of Si NS size distribution from the extinction spectrum, 6. Photographs of Si NSs monolayers on water, 7. Angle dependence of specular reflectance spectra of Si NSs monolayers, 8. Relation between SiO_2 thickness and oxidation duration in Si wafer, 9. Calculated scattering cross section spectra of single Si NS

core/silica shell NS, 10. Total reflectance spectra of Si NSs monolayers before and after oxidation, and 11. Calculated reflectance spectra of hexagonal close-packed structure of Si NS core/silica shell NSs (PDF).

AUTHOR INFORMATION

Corresponding Authors

Minoru Fujii Department of Electrical and Electronic Engineering, Graduate School of Engineering, Kobe University, 1-1 Rokkodai, Nada, Kobe 657-8501, Japan

e-mail: fujii@eedept.kobe-u.ac.jp

Hiroshi Sugimoto Department of Electrical and Electronic Engineering, Graduate School of Engineering, Kobe University, 1-1 Rokkodai, Nada, Kobe 657-8501, Japan

e-mail: sugimoto@eedept.kobe-u.ac.jp

Authors

Haruki Tanaka Department of Electrical and Electronic Engineering, Graduate School of Engineering, Kobe University, 1-1 Rokkodai, Nada, Kobe 657-8501, Japan

Shinnosuke Hotta Department of Electrical and Electronic Engineering, Graduate School of Engineering, Kobe University, 1-1 Rokkodai, Nada, Kobe 657-8501, Japan

Tatsuki Hinamoto Department of Electrical and Electronic Engineering, Graduate School of Engineering, Kobe University, 1-1 Rokkodai, Nada, Kobe 657-8501, Japan

Author Contributions

The manuscript was written through contributions of all authors. All authors have given approval to the final version of the manuscript.

ACKNOWLEDGMENT

This work is partially supported by JSPS KAKENHI, Grant Number 18KK0141, 21H01748, 21H01782 and 22K18949 and JST FOREST Program, Grant Number JPMJFR213L.

References

(1) Evlyukhin, A. B.; Novikov, S. M.; Zywietz, U.; Eriksen, R. L.; Reinhardt, C.; Bozhevolnyi, S. I.; Chichkov, B. N. Demonstration of Magnetic Dipole Resonances of Dielectric Nanospheres in the Visible Region. *Nano Lett.* **2012**, *12* (7), 3749–3755. https://doi.org/10.1021/nl301594s.

(2) Kuznetsov, A. I.; Miroshnichenko, A. E.; Fu, Y. H.; Zhang, J.; Luk'yanchuk, B. Magnetic Light. *Sci. Rep.* **2012**, *2* (1), 492. https://doi.org/10.1038/srep00492.

(3) Baek, K.; Kim, Y.; Mohd-Noor, S.; Hyun, J. K. Mie Resonant Structural Colors. *ACS Appl. Mater. Interfaces* **2020**, *12* (5), 5300–5318. https://doi.org/10.1021/acsami.9b16683.

(4) Kuznetsov, A. I.; Miroshnichenko, A. E.; Brongersma, M. L.; Kivshar, Y. S.; Luk'yanchuk, B. Optically Resonant Dielectric Nanostructures. *Science (80-.).* **2016**, *354* (6314), aag2472. https://doi.org/10.1126/science.aag2472.

(5) Sugimoto, H.; Fujii, M. Colloidal Mie Resonators for All-Dielectric Metaoptics. *Adv. Photonics Res.* **2021**, *2* (4), 2000111. https://doi.org/10.1002/adpr.202000111.

(6) De Marco, M. L.; Semlali, S.; Korgel, B. A.; Barois, P.; Drisko, G. L.; Aymonier, C. Silicon-Based Dielectric Metamaterials: Focus on the Current Synthetic Challenges. *Angew. Chemie - Int. Ed.* **2018**, *57* (17), 4478–4498. https://doi.org/10.1002/anie.201709044.

(7) Fu, Y. H.; Kuznetsov, A. I.; Miroshnichenko, A. E.; Yu, Y. F.; Luk'yanchuk, B. Directional Visible Light Scattering by Silicon Nanoparticles. *Nat. Commun.* **2013**, *4* (1), 1527. https://doi.org/10.1038/ncomms2538.

(8) Jain, P. K.; Lee, K. S.; El-Sayed, I. H.; El-Sayed, M. A. Calculated Absorption and Scattering Properties of Gold Nanoparticles of Different Size, Shape, and Composition: Applications in Biological Imaging and Biomedicine. *J. Phys. Chem. B* **2006**, *110* (14), 7238–7248. https://doi.org/10.1021/jp057170o.

(9) Cobley, C. M.; Skrabalak, S. E.; Campbell, D. J.; Xia, Y. Shape-Controlled Synthesis of Silver Nanoparticles for Plasmonic and Sensing Applications. *Plasmonics* **2009**, *4* (2), 171–179. https://doi.org/10.1007/s11468-009-9088-0.

(10) Sugimoto, H.; Okazaki, T.; Fujii, M. Mie Resonator Color Inks of Monodispersed and Perfectly Spherical Crystalline Silicon Nanoparticles. *Adv. Opt. Mater.* **2020**, *8* (12), 2000033. https://doi.org/10.1002/adom.202000033.

(11) Okazaki, T.; Sugimoto, H.; Hinamoto, T.; Fujii, M. Color Toning of Mie Resonant Silicon Nanoparticle Color Inks. *ACS Appl. Mater. Interfaces* **2021**, *13* (11), 13613–13619. https://doi.org/10.1021/acsami.1c01692.

(12) Yang, W.; Xiao, S.; Song, Q.; Liu, Y.; Wu, Y.; Wang, S.; Yu, J.; Han, J.; Tsai, D.-P. All-Dielectric Metasurface for High-Performance Structural Color. *Nat. Commun.* **2020**, *11* (1), 1864. https://doi.org/10.1038/s41467-020-15773-0.

(13) Dong, Z.; Ho, J.; Yu, Y. F.; Fu, Y. H.; Paniagua-Dominguez, R.; Wang, S.; Kuznetsov, A. I.; Yang, J. K. W. Printing Beyond SRGB Color Gamut by Mimicking Silicon Nanostructures in Free-Space. *Nano Lett.* **2017**, *17* (12), 7620–7628. https://doi.org/10.1021/acs.nanolett.7b03613.

(14) Nagasaki, Y.; Hotta, I.; Suzuki, M.; Takahara, J. Metal-Masked Mie-Resonant Full-Color Printing for Achieving Free-Space Resolution Limit. *ACS Photonics* **2018**, *5* (9), 3849–3855. https://doi.org/10.1021/acsphotonics.8b00895.

(15) Nagasaki, Y.; Suzuki, M.; Takahara, J. All-Dielectric Dual-Color Pixel with Subwavelength Resolution. *Nano Lett.* **2017**, *17* (12), 7500–7506. https://doi.org/10.1021/acs.nanolett.7b03421.

(16) Proust, J.; Bedu, F.; Gallas, B.; Ozerov, I.; Bonod, N. All-Dielectric Colored Metasurfaces with Silicon Mie Resonators. *ACS Nano* **2016**, *10* (8), 7761–7767. https://doi.org/10.1021/acsnano.6b03207.

(17) Kumar, K.; Duan, H.; Hegde, R. S.; Koh, S. C. W.; Wei, J. N.; Yang, J. K. W. Printing Colour at the Optical Diffraction Limit. *Nat. Nanotechnol.* **2012**, *7* (9), 557–561. https://doi.org/10.1038/nnano.2012.128.

(18) Tan, S. J.; Zhang, L.; Zhu, D.; Goh, X. M.; Wang, Y. M.; Kumar, K.; Qiu, C. W.; Yang, J. K. W. Plasmonic Color Palettes for Photorealistic Printing with Aluminum Nanostructures. *Nano Lett.* **2014**, *14* (7), 4023–4029. https://doi.org/10.1021/nl501460x.

(19) Clausen, J. S.; Højlund-Nielsen, E.; Christiansen, A. B.; Yazdi, S.; Grajower, M.; Taha, H.; Levy, U.; Kristensen, A.; Mortensen, N. A. Plasmonic Metasurfaces for Coloration of Plastic Consumer Products. *Nano Lett.* **2014**, *14* (8), 4499–4504. https://doi.org/10.1021/nl5014986.

(20) Zhu, X.; Vannahme, C.; Højlund-Nielsen, E.; Mortensen, N. A.; Kristensen, A. Plasmonic Colour Laser Printing. *Nat. Nanotechnol.* **2016**, *11* (4), 325–329. https://doi.org/10.1038/nnano.2015.285.

(21) Kim, M.; Kim, I.; Jang, J.; Lee, D.; Nam, K. T.; Rho, J. Active Color Control in a Metasurface by Polarization Rotation. *Appl. Sci.* **2018**, *8* (6), 33–35. https://doi.org/10.3390/app8060982.

(22) González-Alcalde, A. K.; Rojas-Martinez, I. Y.; Reyes-Coronado, A. Brewster Effect in Random and Periodic High-Refractive-Index Metasurfaces. *Opt. Commun.* **2022**, *521* (April), 128597. https://doi.org/10.1016/j.optcom.2022.128597.

(23) Razmjooei, N.; Ko, Y. H.; Simlan, F. A.; Magnusson, R. Resonant Reflection by Microsphere Arrays with AR-Quenched Mie Scattering. *Opt. Express* **2021**, *29* (12), 19183. https://doi.org/10.1364/OE.427982.

(24) Vynck, K.; Pacanowski, R.; Agreda, A.; Dufay, A.; Granier, X.; Lalanne, P. The Visual Appearances of Disordered Optical Metasurfaces. *Nat. Mater.* **2022**, *21* (9), 1035–1041. https://doi.org/10.1038/s41563-022-01255-9.

(25) Wray, P. R.; Atwater, H. A. Light–Matter Interactions in Films of Randomly Distributed Unidirectionally Scattering Dielectric Nanoparticles. *ACS Photonics* **2020**, *7* (8), 2105–2114. https://doi.org/10.1021/acsphotonics.0c00545.

(26) Li, L.; Niu, J.; Shang, X.; Chen, S.; Lu, C.; Zhang, Y.; Shi, L. Bright Field Structural Colors in Silicon-on-Insulator Nanostructures. *ACS Appl. Mater. Interfaces* **2021**, *13* (3), 4364–4373. https://doi.org/10.1021/acsami.0c19126.

(27) Jang, J.; Badloe, T.; Yang, Y.; Lee, T.; Mun, J.; Rho, J. Spectral Modulation through the Hybridization of Mie-Scatterers and Quasi-Guided Mode Resonances: Realizing Full and Gradients of Structural Color. *ACS Nano* **2020**, *14* (11), 15317–15326. https://doi.org/10.1021/acsnano.0c05656.

(28) Lee, T.; Kim, J.; Koirala, I.; Yang, Y.; Badloe, T.; Jang, J.; Rho, J. Nearly Perfect Transmissive Subtractive Coloration through the Spectral Amplification of Mie Scattering

and Lattice Resonance. *ACS Appl. Mater. Interfaces* **2021**, *13* (22), 26299–26307. https://doi.org/10.1021/acsami.1c03427.

(29) Eslamisaray, M. A.; Wray, P. R.; Lee, Y.; Nelson, G. M.; Ilic, O.; Atwater, H. A.; Kortshagen, U. R. A Single-Step Bottom-up Approach for Synthesis of Highly Uniform Mie-Resonant Crystalline Semiconductor Particles at Visible Wavelengths. *Nano Lett.* **2023**, *23* (5), 1930–1937. https://doi.org/10.1021/acs.nanolett.2c05084.

(30) Wray, P. R.; Eslamisaray, M. A.; Nelson, G. M.; Ilic, O.; Kortshagen, U. R.; Atwater, H. A. Broadband, Angle- and Polarization-Invariant Antireflective and Absorbing Films by a Scalable Synthesis of Monodisperse Silicon Nanoparticles. *ACS Appl. Mater. Interfaces* **2022**, *14* (20), 23624–23636. https://doi.org/10.1021/acsami.2c03263.

(31) Shigeta, M.; Hirayama, Y.; Ghedini, E. Computational Study of Quenching Effects on Growth Processes and Size Distributions of Silicon Nanoparticles at a Thermal Plasma Tail. *Nanomaterials* **2021**, *11* (6), 1370. https://doi.org/10.3390/nano11061370.

(32) Harris, J. T.; Hueso, J. L.; Korgel, B. A. Hydrogenated Amorphous Silicon (a-Si:H) Colloids. *Chem. Mater.* **2010**, *22* (23), 6378–6383. https://doi.org/10.1021/cm102486w.

(33) Shi, L.; Harris, J. T.; Fenollosa, R.; Rodriguez, I.; Lu, X.; Korgel, B. A.; Meseguer, F. Monodisperse Silicon Nanocavities and Photonic Crystals with Magnetic Response in the Optical Region. *Nat. Commun.* **2013**, *4* (May), 1–7. https://doi.org/10.1038/ncomms2934.

(34) Zhang, C.; Xu, Y.; Liu, J.; Li, J.; Xiang, J.; Li, H.; Li, J.; Dai, Q.; Lan, S.; Miroshnichenko, A. E. Lighting up Silicon Nanoparticles with Mie Resonances. *Nat. Commun.* **2018**, *9* (1), 2964. https://doi.org/10.1038/s41467-018-05394-z.

(35) Xiang, J.; Chen, J.; Dai, Q.; Tie, S.; Lan, S.; Miroshnichenko, A. E. Modifying Mie Resonances and Carrier Dynamics of Silicon Nanoparticles by Dense Electron-Hole Plasmas. *Phys. Rev. Appl.* **2020**, *13* (1), 014003. https://doi.org/10.1103/PhysRevApplied.13.014003.

(36) Makarov, S. V.; Petrov, M. I.; Zywietz, U.; Milichko, V.; Zuev, D.; Lopanitsyna, N.; Kuksin, A.; Mukhin, I.; Zograf, G.; Ubyivovk, E.; Smirnova, D. A.; Starikov, S.; Chichkov, B. N.; Kivshar, Y. S. Efficient Second-Harmonic Generation in Nanocrystalline Silicon Nanoparticles. *Nano Lett.* **2017**, *17* (5), 3047–3053. https://doi.org/10.1021/acs.nanolett.7b00392.

(37) Yan, J.; Liu, P.; Lin, Z.; Wang, H.; Chen, H.; Wang, C.; Yang, G. Directional Fano Resonance in a Silicon Nanosphere Dimer. *ACS Nano* **2015**, *9* (3), 2968–2980. https://doi.org/10.1021/nn507148z.

(38) Li, C.-Q.; Zhang, C.-Y.; Huang, Z.-S.; Li, X.-F.; Dai, Q.-F.; Lan, S.; Tie, S.-L. Assembling of Silicon Nanoflowers with Significantly Enhanced Second Harmonic Generation Using Silicon Nanospheres Fabricated by Femtosecond Laser Ablation. *J. Phys. Chem. C* **2013**, *117* (46), 24625–24631. https://doi.org/10.1021/jp408865p.

(39) Kustov, P.; Petrova, E.; Nazarov, M.; Gilmullin, A.; Sandomirskii, M.; Ponkratova, E.; Yaroshenko, V.; Ageev, E.; Zuev, D. Mie-Resonant Silicon Nanoparticles for Physically Unclonable Anti-Counterfeiting Labels. *ACS Appl. Nano Mater.* **2022**, *5* (8), 10548–10559. https://doi.org/10.1021/acsanm.2c01878.

(40) Chaâbani, W.; Proust, J.; Movsesyan, A.; Béal, J.; Baudrion, A.-L.; Adam, P.-M.; Chehaidar, A.; Plain, J. Large-Scale and Low-Cost Fabrication of Silicon Mie Resonators. *ACS Nano* **2019**, *13* (4), 4199–4208. https://doi.org/10.1021/acsnano.8b09198.

(41) Russo, L.; Colangelo, F.; Cioffi, R.; Rea, I.; Stefano, L. De. A Mechanochemical Approach to Porous Silicon Nanoparticles Fabrication. *Materials (Basel).* **2011**, *4* (6), 1023–1033. https://doi.org/10.3390/ma4061023.

(42) Negoro, H.; Sugimoto, H.; Fujii, M. Helicity-Preserving Optical Metafluids. *Nano Lett.* **2023**, *23* (11), 5101–5107. https://doi.org/10.1021/acs.nanolett.3c01026.

(43) Hinamoto, T.; Hotta, S.; Sugimoto, H.; Fujii, M. Colloidal Solutions of Silicon Nanospheres toward All-Dielectric Optical Metafluids. *Nano Lett.* **2020**, *20* (10), 7737–7743. https://doi.org/10.1021/acs.nanolett.0c03295.

(44) Sugimoto, H.; Fujii, M. Broadband Dielectric-Metal Hybrid Nanoantenna: Silicon Nanoparticle on a Mirror. *ACS Photonics* **2018**, *5* (5), 1986–1993. https://doi.org/10.1021/acsphotonics.7b01461.

(45) Zhao, X.; Li, J.; Liu, Y.; Zhang, Y.; Qu, J.; Qi, T. Preparation and Mechanism of TiO2-Coated Illite Composite Pigments. *Dye. Pigment.* **2014**, *108*, 84–92. https://doi.org/10.1016/j.dyepig.2014.04.022.

(46) Palik, E. D. *Handbook of Optical Constants of Solids*; 2012; Vol. 1. https://doi.org/10.1016/C2009-0-20920-2.

(47) Bohren, C. F. *Absorption and Scattering of Light by Small Particles*; 1983. https://doi.org/10.1088/0031-9112/35/3/025.

(48) Le Ru, E. C.; Etchegoin, P. G. *Principles of Surface-Enhanced Raman Spectroscopy*; 2009. https://doi.org/10.1016/B978-0-444-52779-0.X0001-3.

TOC graphic